PROCEEDINGS OF SCIENCE

The interplay of ice-firn model and station calibration in RNO-G

Bob Oeyen[a,*] **for the RNO-G Collaboration**
(a complete list of authors can be found at the end of the proceedings)

[a] *Department Physics and Astronomy - Ghent University,*
Proeftuinstraat 86, 9000 Gent, Belgium
E-mail: bob.oeyen@ugent.be

In-ice radio neutrino detectors, such as the newly constructed and operational Radio Neutrino Observatory in Greenland (RNO-G), rely on ice models to understand the in-ice signal propagation. Most often the ice is approximated in first order by a single exponential profile because it allows for computationally fast signal propagation. However, such models do not encompass the whole complexity of the ice, which may lead to systematic uncertainties. This is especially true for the upper part of the ice (the firn) where most of the RNO-G antennas are situated. Therefore, we developed a new refractive index model of the ice at Summit Station which can be used in both simulation and analysis. This contribution shows how both density data and signals from various known radio sources, such as the on board radio pulser and weather balloons, can lead to a more accurate description of the ice. This revised ice model results in a better understanding of signal arrival times, thus resulting in an improved station calibration in RNO-G. In the future we expect to bridge the gap even further by performing dedicated and more rigorous ice measurement in the field.

The 38th International Cosmic Ray Conference (ICRC2023)
26 July – 3 August, 2023
Nagoya, Japan

*Speaker

PoS(ICRC2023)1042

Introduction

To understand, analyse and reconstruct signals of in-ice radio neutrino detectors, such as the Radio Neutrino Observatory in Greenland (RNO-G) [1], a good description of signal propagation is needed. Ray tracing based on a single exponential ice model is computationally fast but lacks the complexity of glacier ice inducing systematic errors. Therefore, we designed a new polynomial exponential ice model based of density and calibration data to alleviate this. These proceedings report on the construction and verification of this ice model exploiting the RNO-G station calibration.

1. From simple to complex index of refraction models

An accurate model of the optical properties of the ice is important for a good understanding of the signal propagation. Several complex phenomena can occur, such as birefringence or reflective layers, but the most basic feature is the refractive index. To first order, the index of refraction of glacial ice is often described by a single exponential profile as its analytically solvable ray paths allow fast computation. However, when comparing this model to the data at Summit Station, discrepancies are clearly visible. Therefore, the exponential polynomial model was devised by adding higher order correction to this basic model, which seems to work better.

1.1 Single exponential profiles — Schytt's emirical equation

Because ice is not a homogeneous medium (especially in the upper layers called the firn), the refractive index of ice will differ from place to place. In general it is understood that the index of refraction will continuously and asymptotically increase with depth: from the surface down through the firn, the refractive index increases towards a more uniform regime in the deep homogeneous bulk ice. A first general description was given by Schytt in the form of a exponential profile.

This general first order profile of the refractive index can be explained due to the close relationship between the refractive index and the density of the medium. In glacier ice the refractive index n en density ρ are often connected through a linear expression [2]:

$$n = 1 + \rho \cdot 0.851 \text{cm}^3/\text{g} \tag{1}$$

Additionally, it can naturally be understood that the density of ice increases with depth due to the stress of the overlying weight of the snow and ice. One of the first models describing density as a function of depth was introduced by Schytt, who empirically fitted (in first order) a single exponential profile to density data gathered at Maudheim [3].

$$\rho(z) = \rho_{ice} - (\rho_{ice} - \rho_{snow}) \cdot \exp\left(\frac{(z - \Delta z)}{z_0}\right) \tag{2}$$

From this equation, mainly the scaling depth z_0 needs to be fitted for as the density of bulk glacial ice ρ_{ice} and the snow ρ_{snow} are known. Because of the relation of Eq. 1 between density and refractive index, the profile of the index of refraction is also described in first order by a single exponential.

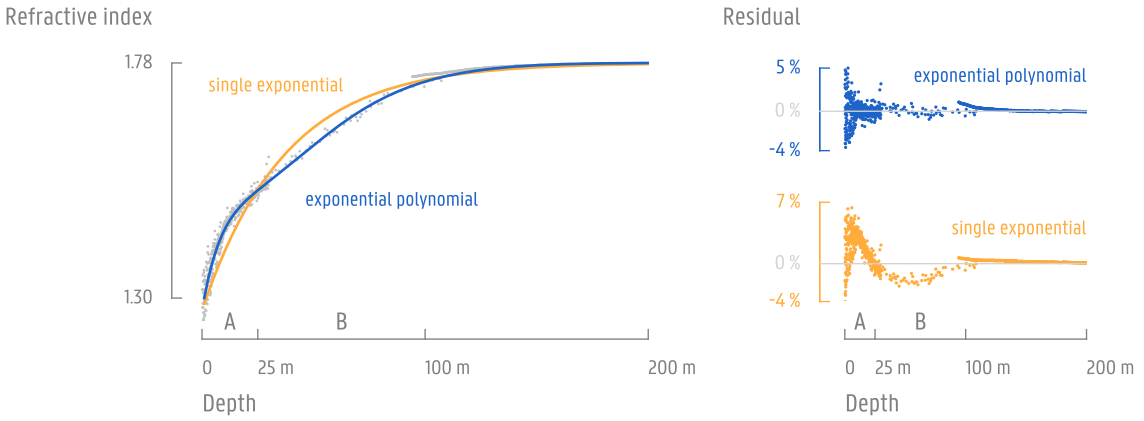

Figure 1: The higher order corrections of the exponential polynomial mitigate the overestimation and underestimation of the single exponential model in respectively region A and B. Data points of the refractive index correspond to the conversion (using Eq. 1) of historical density data obtained with different methods[5–7] at Summit Station, which mostly agree with each other except around ±100 m.

1.2 Polynomial exponential profile — higher order corrections on Schytt

The single exponential profile of Schytt exposes the general behaviour of the refractive index but ignores subtle differences which can be captured by the higher order corrections of the exponential polynomial. When fitting Schytt's model to historical data from Summit Station, it is clear this works to some extent however two major region of discrepancy can be can be recognised (Fig. 1): region A from 0 m ~ 25 m where the model undershoot the data, and region B from 25 m ~ 100 m where the model overshoots the data. To mitigate this we introduce higher order correction to the single exponential profile up to five orders, resulting in a 5^{th} degree exponential polynomial:

$$\rho(z) = \sum_{i=0}^{5} a_i \cdot \exp^i \left(\frac{z - \Delta z}{z_0} \right) \tag{3}$$

with $a_0 = \rho_{ice}$. The higher order corrections of this new model largely eliminate the biases in region A and B, leaving only statistical fluctuations (Fig. 1). Note that this model is still a scalar field and does not depend on signal direction (birefringence), which is justified for our purpose as birefringence at Summit Station is negligible for short paths, especially for vertical signals [4].

2. Verifying ice models using station calibration

The initial surveyed antenna positions can serve as a starting point for extracting information about the accuracy of ice models. For calibrating antenna positions, the surveyed positions are fine-tuned to fit the timing of known radio signals [8]. Unfortunately, signal timing depends on both travel distance and the refractive index of ice, causing possible biases in the ice model (Sec. 1.2) to be converted into position biases, entangling the two. However, if the calibration process pushes or pulls the antenna systematically in one direction, this can indicate a problem with the ice model.

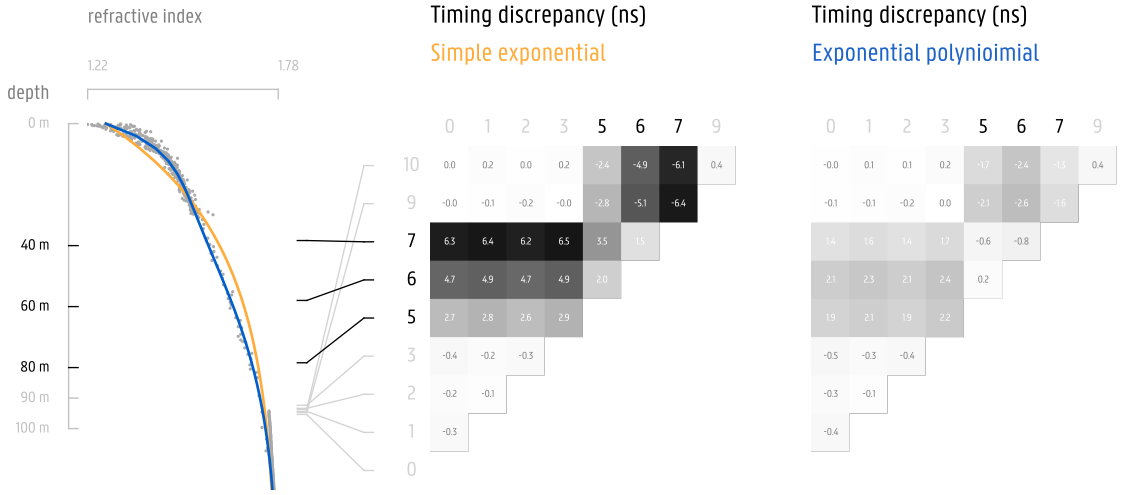

Figure 2: The exponential polynomial fit describes the inter-antenna timing for antenna pairs better than the single exponential fit, especially for the intermediate antennas (5,6,7) located in depth region B (Fig. 1).

The timing data from pulsar runs seem to favour the exponential polynomial ice profile over the single exponential profile for RNO-G, due to an improved timing for the intermediate antennas. Because the initial position of pulsar and antennas are known to some extend, they constrain the possible ice models in a way. On one hand, the inter-antenna timing of an antenna pair can be measured by cross-correlating signals to templates and each other (page 4). On the other hand, this timing is also predicted by the ice model. The difference between these two time measures is an indication for the accuracy of the position and possible biases of the ice model. The inter-antenna timing for the deep part of the RNO-G stations (phased array and helper string) does not show immediate problems. However, timings involving an intermediate antenna (antennas between the surface and deep phased array) show a constant bias in one direction for the single exponential model (Fig. 2). This suggest the model does not described well the refractive index in the region of these antennas, which happens to be region B as earlier discussed in Sec. 1.2. When the single exponential is swapped for the exponential polynomial, the biases diminishes and almost disappear between the intermediate antennas themselves. However, between phased array and intermediate antennas the discrepancies remain although smaller.

Finding inter-antenna signal timing

The timing offset of a recorded signal between two antennas can be deduced from the peak(s) of the cross-correlation of the two voltage traces. However, when the signal-to-noise ratio is low, this technique will not work well. To overcome this, traces are first cross-correlated to a template of the incoming signal. Finally, these template cross-correlations are cross-correlated to each other and from its peak(s) the inter-antenna timing is derived.

3. Probing the deep firn using weather balloons

An independent measurement of the refractive index at the RNO-G phased array can be obtained from signals of weather balloons. When approximating the incoming balloon's signal as a plane wave, the local refractive index n is connected following three variable: inter-antenna timing Δt, inter-antenna position Δz, and the signal arrival zenith angle θ.

3.1 The method — plane wave fit of weather balloon data and signals

Using the geometry of a plane wave, the refractive index can be calculated from the weather balloon data and signal considering some assumptions. The assumptions can be justified by making smart selections about which balloons and antennas to include in the search. These carefully selected event can then be used to determine the refractive index performing a linear regression to the equation provided by the problem's geometry.

For the plane wave approximation to work, the following three assumptions are made and justified: 1| the signal arrival direction is the same at each antenna, 2| the timing differences between antennas are only the result of the local difference in travel distance, and 3| The signal's velocity, and therefore also the refractive index, is the same at all antennas. To accommodate these assumption, the search only uses the RNO-G phased array in combination with distant overhead sources. Firstly, the phased array is located deep in the firn and channel spacing is at most 5 m, thus the refractive index can be assumed to middle out in its centre with only small differences between antennas. Secondly, signals from distant source (such as weather balloons) reach the antennas in nearly the same direction because the antennas can almost be seen as a single point from far away due to the small inter-antenna spacing. Lastly, near-to-overhead flying balloons are most insensitive to the overlaying, ice meaning timing difference are a result of the local antenna geometry (Sec. 3.2).

The geometry of the plane wave approximation allows for a simple connection between the three known variables and the refractive index in the form of Eq. 4. As a signal travels under zenith angle θ_{sgl} towards a vertical antenna pair with spacing Δz, it reaches antenna A first but still needs to travel a certain distance $d = \cos(\theta) \cdot \Delta z$ towards antenna B (Fig. 3). This will result in a timing difference between the two antennas, which depends on the spacing and the local signal velocity c_n given by the local refractive index. The geometry thus connects the timing, spacing, zenith to the refractive index through the equation:

$$c \cdot \Delta t = n \cdot \cos(\theta) \cdot \Delta z \tag{4}$$

Since θ_{sgl} is considered to be the same for each antenna pair during one event, the data points $(\Delta z, \Delta t)$ can be combined into one fit for n with a linear regression.

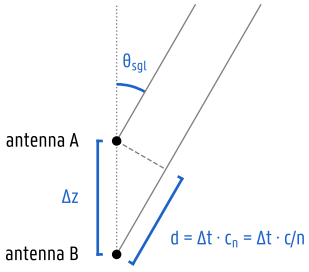

Figure 3: The plane wave geometry relates the inter-antenna timing Δt to the inter-antenna spacing Δz and the signal zenith θ_{sgl} through the refractive index n

3.2 The variables — extracting measurements from balloon, event and detector data

To use the plane wave method described in the previous section (Sec. 3.1), the inter-antenna timing, inter-antenna spacing, and incoming signal zenith angle need to be extracted out of the data. This is achieved respectively through event signal cross-correlations, antenna field measurements, and balloon and station GPS data. For this data we are able to extract the refractive index.

The inter-antenna timing of a recorded signal between two antennas can be found by selecting the right peak in the cross-correlation. The signal timing difference of an antenna pair can be measured by cross-correlating both recorded signals to templates and each other (page 4). However, these inter-antenna timings have a periodic ambiguity ($\Delta t \pm k/f_{sgl}$, with k an integer and f_{sgl} = 403 MHz the signal frequency) as the incoming signal is a continuous wave. Luckily, for an inter-antenna spacing of a few signal wavelengths, this ambiguity can be overcome by determining a expectation window based on the signal's zenith and a crude estimate of the local refractive index.

For near-to-overhead flying weather balloons ($\theta_{bln} < 5°$), the signal's zenith angle θ_{sgl} can be approximated by the balloon's zenith angle θ_{bln}. Balloon signals travel through the air downwards into the ice and are refracted at the boundary towards the vertical, after which they bend even further towards the vertical due to an always increasing index of refraction. The zenith of the incoming signal at the antenna θ_{sgl} is thus always smaller than the zenith of the balloon's position relative to that antenna θ_{bln}. Thus, using the balloon's zenith angle (calculated from balloon and detector GPS data) as a proxy for the signal's zenith angle will always result in an overestimation of the local refractive index, resulting in a systematic uncertainty. However, the signal's direction is mainly vertical for balloons flying near to overhead so refraction is small, meaning the signal zenith can be approximated by the balloon zenith ($\theta_{sgl} \approx \theta_{bln}$) without a too big overestimation. Limiting the analysis to weather balloons with zenith angles smaller than 5° ensure the systematic uncertainty on the refractive index is at most −1.0% (Fig. 4). Additionally, as the refraction is less pronounced for the signals of these balloons, one can safely assume that the signal paths are the same in the overlaying ice and paths only differ because of the local inter-antenna spacing, which accommodates assumption 3| made in the previous section (Sec. 3.1).

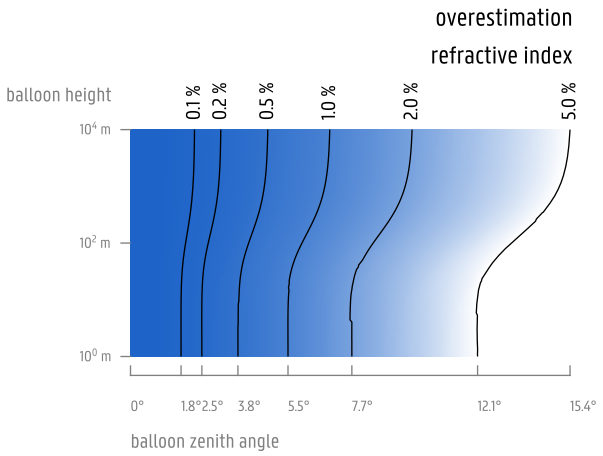

Figure 4: Putting a cut of < 4.5° on the balloon's zenith and > 500 m on the balloon's height, limits the systematic overestimation of the refractive index to 0.5%, as the overestimation increases with balloon's zenith and decreases with balloon's height.

The inter-antenna spacing is obtained directly from field measurements during deployment and is well known in contrast to the absolute position. The absolute measured antenna position can vary up to a meter because of a not well defined absolute reference point. However, as the reference point is the same for all antennas on the same string and its relative position to the antennas is well known, the inter-antenna spacing on the same string only varies up to ±5 cm.

3.3 The results — refractive index measurement at station 11

As a prove of concept of the described procedure, we determined the index of refraction of ice at the phased array of RNO-G station 11 to be 1.736 ± 0.002 (stat). This result lies between what is expected by the simple exponential model and the exponential polynomial, but it is compatible with both within two standard deviations. However, this measurement was obtained through the analysis of one specific balloon flight, thus results may vary between events and stations.

After extracting the necessary data to perform the procedure, the index of refraction could be determined to an precision of 0.12 % including the correction for overestimation. The inter-antenna timing and spacing data form a well behaved direct proportionality to which Eq. 4 could be fitted with great accuracy by (Fig. 5). Using the balloon's zenith angle of $\theta_{bln} = 3.11° \pm 0.05°$ the fit can be resolved for the index of refraction, and a value of $n = 1.740 \pm 0.002$ is found. However, as discussed in Sec. 3.2, this is is an overestimation due to the approximation $\theta_{sgl} \approx \theta_{bln}$. From simulation, this overestimation seems to be more or less independent from the ice model with a value of $0.20\% \pm 0.02\%$ for this specific event. Correcting for this overestimation, a refractive index of 1.736 ± 0.002 at the phased array is obtained. Note that this value is associated with the centre

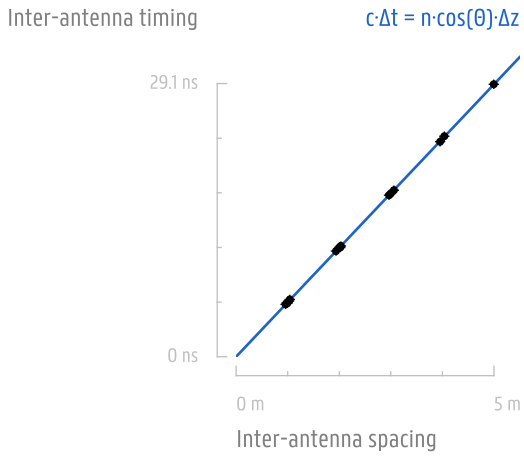

Figure 5: The inter-antenna timing Δt is directly proportional to the inter-antenna spacing Δz. With the balloon's zenith $\theta_{bln} = 3.11° \pm 0.05°$ the linear regression results in a index of refractive $n = 1.740 \pm 0.002$ without systematic correction.

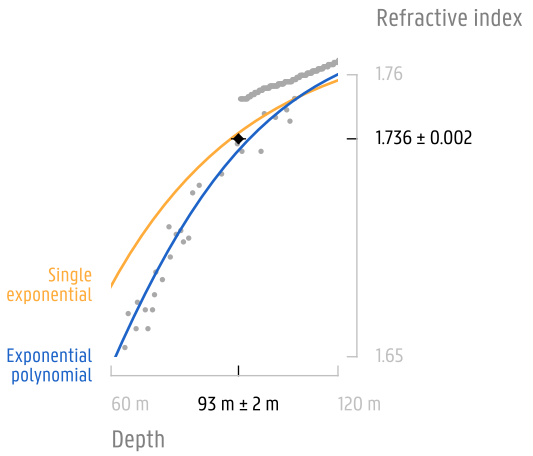

Figure 6: The determined index of refraction follows the results obtained from density data, and it is compatible with both the single exponential model and the exponential polynomial model within two standard deviations.

of the phased array at 93 ± 2 m depth. There is a slight spread in refractive index from the top to the bottom of the phased array but this will middle out in the centre as locally the change in refractive index can be assumed to be linear. Comparing this result to refractive index measurement of the bulk ice of 1.778 ± 0.006 [9], this also seems to support the validity of Eq. 1

This results is obtained using the phased array of a specific RNO-G station for one specific weather balloon flight, meaning variation for different events or station locations are not taken into account. On the 24$^{\text{th}}$ of July 2022, this weather balloon was launched at Summit Station, after which is flew passed RNO-G station 11 within a minimal zenith angle of $\theta = 3.11° \pm 0.05°$. A clear peak at the balloon's frequency f_{sgl} was identified in the power spectrum of the recorded event at this station, resulting in an accurate timing fitting and thus an accurate refractive index measurement. However, the accuracy (and result to some extend) may vary from event to event due to higher or lower signal-to-noise ratio. Furthermore, the result may vary from station to station as it is unclear how uniform the vertical profile is in horizontal displacements.

Conclusion

The exponential polynomial ice model, with its higher order corrections to the single exponential, improves the inter-antenna timing prediction for the deep calibration pulsar. Furthermore, this new model is consistent with an independent measurement of the index of refraction at the phased array of 1.736 ± 0.002. Therefore, these results indicate the polynomial exponential is an improved description of the glacial ice at Summit Station. However, there are still some discrepancies between the phased array and the intermediate channel, and there might be more variations between station locations and events which isn't included in this analysis yet. Additionally, a direct measurement of the refractive index in function of depth (partially planned for RNO-G [8]) would also be helpful to further verify the relation between density and refractive index (Eq. 1), as this is an empirical relation based on data from another site and the relation might not be universal.

References

[1] **RNO-G** Collaboration, J. A. Aguilar *et al. JINST* **16** no. 03, (2021) P03025. [Erratum: JINST 18, E03001 (2023)].

[2] E. S. Robin, G. De Q. and J. T. Bailey *Philosophical Transactions of the Royal Society of London. Series A, Mathematical and Physical Sciences* **265** no. 1166, (1969) 437–505.

[3] V. Schytt *Norwegian-British-Swedish Antarctic Expedition, 1949-52. Scientific Result* **IV** (1958) 113–151.

[4] **RNO-G** Collaboration, J. A. Aguilar *et al. arXiv* no. 2212.10285, (2022) .

[5] R. L. Hawley, E. M. Morris, and J. R. McConnell *Journal of Glaciology* **54** no. 188, (2008) 839–845.

[6] R. B. Alley and B. R. Koci *Annals of Glaciology* **10** (1988) 1–4.

[7] R. Alley, C. Shuman, D. Meese, A. Gow, K. Taylor, K. Cuffey, J. Fitzpatrick, P. Grootes, *et al. Journal of Geophysical Research: Oceans* **102** no. C12, (1997) 26367–26381.

[8] **RNO-G** Collaboration, C. Welling *et al. Proc. of Science* no. PoS(ICRC2023)1054, (2023) .

[9] **RNO-G** Collaboration, J. A. Aguilar *et al. arXiv* no. 2304.06181, (2023) .

Full Author List: RNO-G Collaboration

J. A. Aguilar[1], P. Allison[2], D. Besson[3], A. Bishop[10], O. Botner[4], S. Bouma[5], S. Buitink[6], W. Castiglioni[8], M. Cataldo[5], B. A. Clark[7], A. Coleman[4], K. Couberly[3], P. Dasgupta[1], S. de Kockere[9], K. D. de Vries[9], C. Deaconu[8], M. A. DuVernois[10], A. Eimer[5], C. Glaser[4], T. Glüsenkamp[4], A. Hallgren[4], S. Hallmann[11], J. C. Hanson[12], B. Hendricks[14], J. Henrichs[11,5], N. Heyer[4], C. Hornhuber[3], K. Hughes[8], T. Karg[11], A. Karle[10], J. L. Kelley[10], M. Korntheuer[1], M. Kowalski[11,15], I. Kravchenko[16], R. Krebs[14], R. Lahmann[5], P. Lehmann[5], U. Latif[9], P. Laub[5], C.-H. Liu[16], J. Mammo[16], M. J. Marsee[17], Z. S. Meyers[11,5], M. Mikhailova[3], K. Michaels[8], K. Mulrey[13], M. Muzio[14], A. Nelles[11,5], A. Novikov[19], A. Nozdrina[3], E. Oberla[8], B. Oeyen[18], I. Plaisier[5,11], N. Punsuebsay[19], L. Pyras[11,5], D. Ryckbosch[18], F. Schlüter[1], O. Scholten[9,20], D. Seckel[19], M. F. H. Seikh[3], D. Smith[8], J. Stoffels[9], D. Southall[8], K. Terveer[5], S. Toscano[1], D. Tosi[10], D. J. Van Den Broeck[9,6], N. van Eijndhoven[9], A. G. Vieregg[8], J. Z. Vischer[5], C. Welling[8], D. R. Williams[17], S. Wissel[14], R. Young[3], A. Zink[5]

[1] Université Libre de Bruxelles, Science Faculty CP230, B-1050 Brussels, Belgium
[2] Dept. of Physics, Center for Cosmology and AstroParticle Physics, Ohio State University, Columbus, OH 43210, USA
[3] University of Kansas, Dept. of Physics and Astronomy, Lawrence, KS 66045, USA
[4] Uppsala University, Dept. of Physics and Astronomy, Uppsala, SE-752 37, Sweden
[5] Erlangen Center for Astroparticle Physics (ECAP), Friedrich-Alexander-University Erlangen-Nürnberg, 91058 Erlangen, Germany
[6] Vrije Universiteit Brussel, Astrophysical Institute, Pleinlaan 2, 1050 Brussels, Belgium
[7] Department of Physics, University of Maryland, College Park, MD 20742, USA
[8] Dept. of Physics, Enrico Fermi Inst., Kavli Inst. for Cosmological Physics, University of Chicago, Chicago, IL 60637, USA
[9] Vrije Universiteit Brussel, Dienst ELEM, B-1050 Brussels, Belgium
[10] Wisconsin IceCube Particle Astrophysics Center (WIPAC) and Dept. of Physics, University of Wisconsin-Madison, Madison, WI 53703, USA
[11] Deutsches Elektronen-Synchrotron DESY, Platanenallee 6, 15738 Zeuthen, Germany
[12] Whittier College, Whittier, CA 90602, USA
[13] Dept. of Astrophysics/IMAPP, Radboud University, PO Box 9010, 6500 GL, The Netherlands
[14] Dept. of Physics, Dept. of Astronomy & Astrophysics, Penn State University, University Park, PA 16801, USA
[15] Institut für Physik, Humboldt-Universität zu Berlin, 12489 Berlin, Germany
[16] Dept. of Physics and Astronomy, Univ. of Nebraska-Lincoln, NE, 68588, USA
[17] Dept. of Physics and Astronomy, University of Alabama, Tuscaloosa, AL 35487, USA
[18] Ghent University, Dept. of Physics and Astronomy, B-9000 Gent, Belgium
[19] Dept. of Physics and Astronomy, University of Delaware, Newark, DE 19716, USA
[20] Kapteyn Institute, University of Groningen, Groningen, The Netherlands

Acknowledgments

We are thankful to the staff at Summit Station for supporting our deployment work in every way possible. We also acknowledge our colleagues from the British Antarctic Survey for embarking on the journey of building and operating the BigRAID drill for our project. We would like to acknowledge our home institutions and funding agencies for supporting the RNO-G work; in particular the Belgian Funds for Scientific Research (FRS-FNRS and FWO) and the FWO programme for International Research Infrastructure (IRI), the National Science Foundation (NSF Award IDs 2118315, 2112352, 211232, 2111410) and the IceCube EPSCoR Initiative (Award ID 2019597), the German research foundation (DFG, Grant NE 2031/2-1), the Helmholtz Association (Initiative and Networking Fund, W2/W3 Program), the University of Chicago Research Computing Center, and the European Research Council under the European Unions Horizon 2020 research and innovation programme (grant agreement No 805486).